Applied Organometallic Chemistry

WILEY

Applied Organometallic Chemistry

FULL PAPER OPEN ACCESS

Electrochemical Performance of a New Triazole Functionalized Ferrocene in Aqueous Redox Flow Batteries

Taha Yasin Eken[1,2] | Gabriel Gonzalez[2] | Pekka Peljo[2] | Gamze Koz[3]

[1]Department of Metallurgical and Materials Engineering, Faculty of Engineering and Natural Sciences, Bursa Technical University, Bursa, Turkey | [2]Department of Mechanical and Materials Engineering, Faculty of Technology, Research Group of Battery Materials and Technologies, University of Turku, Turku, Finland | [3]Department of Chemistry, Faculty of Engineering and Natural Sciences, Bursa Technical University, Bursa, Turkey

Correspondence: Gamze Koz (gamze.koz@btu.edu.tr)

Received: 10 July 2024 | **Revised:** 21 September 2024 | **Accepted:** 24 September 2024

Funding: This work was supported by Turun Yliopisto, Bursa Technical University Scientific Research Fund (231N002), and European Research Council (950038).

Keywords: 1,2,3-triazole | click chemistry | electrochemistry | ferrocene | redox flow battery

ABSTRACT

A new 1,2,3-triazole functionalized ferrocene (1,2,3-TAFc) produced by Cu(I)-catalyzed click reaction was investigated as positive electrolyte for aqueous organic flow batteries (AOFBs). The molecule is highly soluble in 1 M hydrochloric acid and displays high electrochemical reversibility. 1,2,3-TAFc demonstrated good stability during cycling with a low capacity decay (0.011%/cyc, 3.0%/day) and high Coulombic efficiency (99.4%) over 280 cycles when tested in a flow battery at low concentration. This low capacity decay was attributed to the instability of ferrocene. These findings indicate that a stable and water-soluble catholyte for AOFBs can be obtained with structural modifications of 1,2,3-TAFc.

1 | Introduction

Green transformation of our electricity production has become even more essential in recent years due to the global energy crisis and the increasing carbon footprint [1, 2]. The intermittent nature of renewables makes grid-scale energy storage systems necessary. Aqueous organic flow batteries (AOFBs) are a viable option for safe and large-scale energy storage because AOFBs can store the electrical energy produced from renewable sources externally from the battery cell in storage tanks filled with liquid electrolytes. Electricity is stored in redox active organic molecules dissolved in aqueous electrolytes. Crucial parameters such as high solubility, electrochemical potential, and stability can be tuned by modification of the molecular structures [3–7]. Organic species used on the positive side of an optimal AOFB should have high redox potentials while low redox potentials are desirable for the species on the negative side. A variety of derivatives such as quinone, viologens, flavin, alizarin, alloxazine, and phenazine have successfully been reported for the negative side [8–12]; however, the options for the positive side are rather limited to ferrocyanide, some ferrocene (Fc), and 2,2,6,6-tetramethylpiperidine-1-oxyl (TEMPO) derivatives [11, 13–15].

Fc is a redox active molecule displaying a standard potential of ca. 0.4 V versus standard hydrogen electrode (SHE) based on the reversible Fe^{2+}/Fe^{3+} redox couple. However, unsubstituted Fc is not a potential material for AOFBs as it is insoluble in water [16]. Water-soluble Fc derivatives have been obtained by modifying the cyclopentadienyl (Cp) ring, mainly as a quaternary ammonium or a sulfonate salt [11, 13, 17]. The identity and the effect of cation on water solubility and electrochemical performance of Fc sulfonate salts in AORFBs was investigated recently [18–20]. Although several hydrophilic Fc derivatives have been synthesized and reported as candidates for AOFBs, all these materials

Taha Yasin Eken and Gabriel Gonzalez contributed equally.

had some limitations in terms of synthesis procedures such as long reaction times and low total yields after a few reaction steps (see Table S1).

Another limitation of Fc-based electrolytes is the capacity loss during the long-term cycling evaluation, which is mainly caused by the degradation of Fc units. Chen et al. investigated the influence of substituents on molecular stability and proposed a decomposition mechanism that starts with the nucleophilic attack of water to the metallic center [21]. Under neutral conditions, the water molecule donates an electron to the LUMO orbitals of the Fc, resulting in degradation. As nucleophilicity of water mainly depends on the pH of the electrolyte solution, controlling the pH of the solution is a key approach for ensuring long-term stability.

These limitations underscore the necessity for developing Fc derivatives with enhanced solubility, stability, and simpler synthesis routes. To address these challenges, we present the design and synthesis of a novel 1,4-disubstituted-1,2,3-triazole-derived ferrocene (1,2,3-TAFc), which was produced through a straightforward Cu(I)-catalyzed click reaction. 1,2,3-TAFc was highly soluble in 1 M hydrochloric acid (HCl) solution so the electrochemical properties of 1,2,3-TAFc have been investigated in an acidic supporting electrolyte. The chemical and electrochemical characteristics of the 1,2,3-TAFc is demonstrated through nuclear magnetic resonance (NMR) and cyclic voltammetry (CV) analyses for the confirmation of its structure, stability, and electrochemical reversibility. Moreover, the stability of 1,2,3-TAFc was studied in laboratory-scale flow batteries through galvanostatic cycling tests.

2 | Results and Discussion

2.1 | Chemistry

We designed a neutral Fc derivative with an amino functional group and a triazole ring. In acidic electrolyte solution, in situ formed quaternary ammonium and triazolium salts resulted in high water solubility. 1,2,3-TAFc was obtained using one-pot Cu(I) catalyzed azide-alkyne cycloaddition reaction between ethynylferrocene and alkyl azide (Figure 1). 1,2,3-TAFc was synthesized with a modified procedure reported in the literature [22].

The characterization of 1,2,3-TAFc was performed using UV–Vis spectroscopy, Fourier transform infrared spectroscopy (FT-IR), nuclear magnetic resonance spectroscopy (^{1}H NMR, ^{13}C NMR, and HSQC), and high-resolution mass spectrometry (HR-MS). Figure S1 of ESI shows the ^{1}H NMR spectrum of 1,2,3-TAFc with five equivalent aromatic protons as a singlet at 4.07 ppm for the unsubstituted Cp ring. The substituted Cp ring protons were seen as two triplets centered at 4.28 and 4.70 ppm, integrating for two protons each. The characteristic 1,2,3-triazole proton was observed at 7.54 ppm (s, 1H) while the CH_2 protons were recorded at 4.39 and 3.22 ppm (t, 2H) and NH_2 protons appeared at 1.49 ppm as a broad singlet. The heteronuclear single-quantum correlation experiment (HSQC) of 1,2,3-TAFc was also performed to determine the correlated carbon signals.

Solubility is one of the key properties of redox active materials used in AOFBs. Table 1 lists the solubility of the 1,2,3-TAFc in common organic solvents and in 1 M HCl solution. 1,2,3-TAFc was easily dissolved in acidic electrolyte as it was converted to its 1,2,3-triazolium chloride and alkyl ammonium chloride salt in HCl solution. The molecule has a solubility of 1.1 M in HCl solution and the best solubility in non-aqueous solutions are observed in polar aprotic solvents such as *N*,*N*-dimethylformamide (DMF) and dimethyl sulfoxide (DMSO) while it has a lower solubility in polar protic solvents such as alcohols. 1,2,3-TAFc is slightly soluble in water.

TABLE 1 | Solubility of 1,2,3-TAFc in different solvents.

Solvent	Solubility
1 M HCl solution	1.1 M
DMF	0.20 M
DMSO	0.15 M
Methanol	7 mM
Ethanol	5 mM
Dichloromethane	5 mM
Acetonitrile	2 mM
Water	0.9 mM

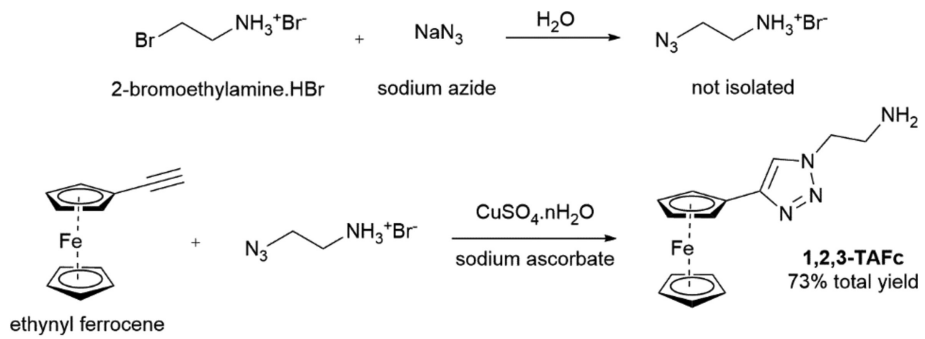

FIGURE 1 | One-pot synthesis and total yield of 1,2,3-TAFc.

2.2 | Cyclic Voltammetry

Standard cyclic voltammetry (CV) experiments were performed in 1 M HCl supporting electrolyte at different scan rates and Randles–Ševčík analysis for 25 mM 1,2,3-TAFc in 1 M HCl are shown in Figure 2. These experiments allow measuring the redox potentials and diffusion coefficients of the molecules of interest and giving preliminary evaluation of the stability and electrochemical kinetics of the species. For further information on how to interpret the voltammetry data, please refer to electrochemistry text books or tutorial reviews [23]. The voltammograms in Figure 2a show a highly reversible redox process occurring at a half-wave potential ($E_{1/2}$) of 0.318 V versus Ag/AgCl in 3 M KCl, corresponding to 0.518 V versus SHE, with peak separation close to 60 mV expected for reversible system with one electron transferred. The half-wave potential is the average of the peak potentials, if the diffusion coefficient of the oxidized and reduced forms is not different. Figure 2b illustrates a linear correlation between the peak current and the square root of the scan rate following the Randles–Ševčík equation. This indicates that the redox reaction of 1,2,3-TAFc is diffusion-controlled. The diffusion coefficient of 1,2,3-TAFc, calculated using the Randles–Ševčík equation (see calculation in the supporting information), is 6.26×10^{-6} cm^2/s. This value is comparable with those reported for other ferrocene-derived organometallic compounds in neutral aqueous solutions as documented in the literature [24, 25].

The CV results for 1,2,3-TAFc at varying concentrations (2–25 mM) are presented in Figure 3, with the corresponding data summarized in Table 2. The results demonstrate that the redox peaks remain well-defined across all concentrations, indicating the high reversibility of the redox couple. As expected from Randles–Ševčík equation, the peak current increases linearly with concentration, reflecting the greater availability of redox-active species.

The ratio of the anodic peak current (I_{PA}) to the cathodic peak current (I_{PC}) (Figure S2) is approximately 1.03, confirming the electrochemical reversibility of 1,2,3-TAFc in an acidic aqueous solution with a scan rate of 100 mV/s in 1 M HCl [26]. The peak current ratios provide insights into the reversibility of the redox process, with values remaining close to 1 at all concentrations, indicating a reversible redox couple. The slight deviations from unity are often attributed to challenges in accurately performing the baseline correction, particularly for the reduction peak.

Continuous cycling over 100 cycles shows no degradation on the time scale of the CV (Figure 4, Figure S3). These figures offer valuable insights into the stability of 1,2,3-TAFc during repeated cycling. At all concentrations, the peak currents remain relatively stable over 100 cycles, indicating good stability and reversibility. However, a slight decrease in peak current is observed at the 25 mM concentration after 100 cycles, which may be due to either degradation of the active material or the accumulation of side reactions at higher concentrations. This suggests that while 25 mM provides a higher initial current, its long-term stability could be compromised, highlighting the need for further optimization of concentration to ensure extended cycling performance.

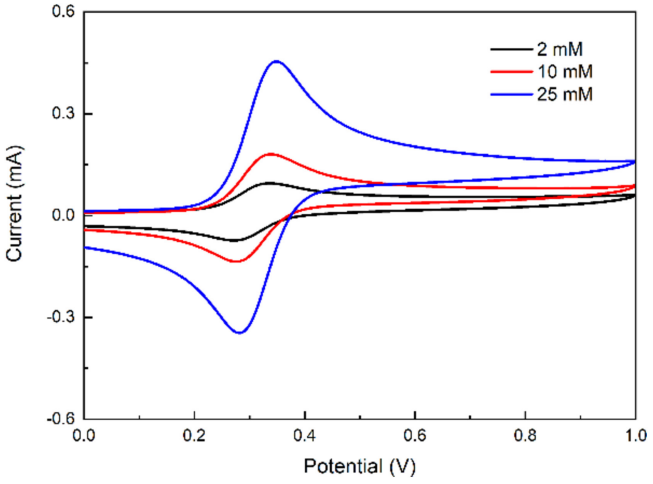

FIGURE 3 | CV results (V vs. Ag/AgCl) of 1,2,3-TAFc at 2, 10, and 25 mM concentrations. The scan rate is 100 mV/s and the supporting solution is 1 M HCl aqueous solution (pH = 0.4).

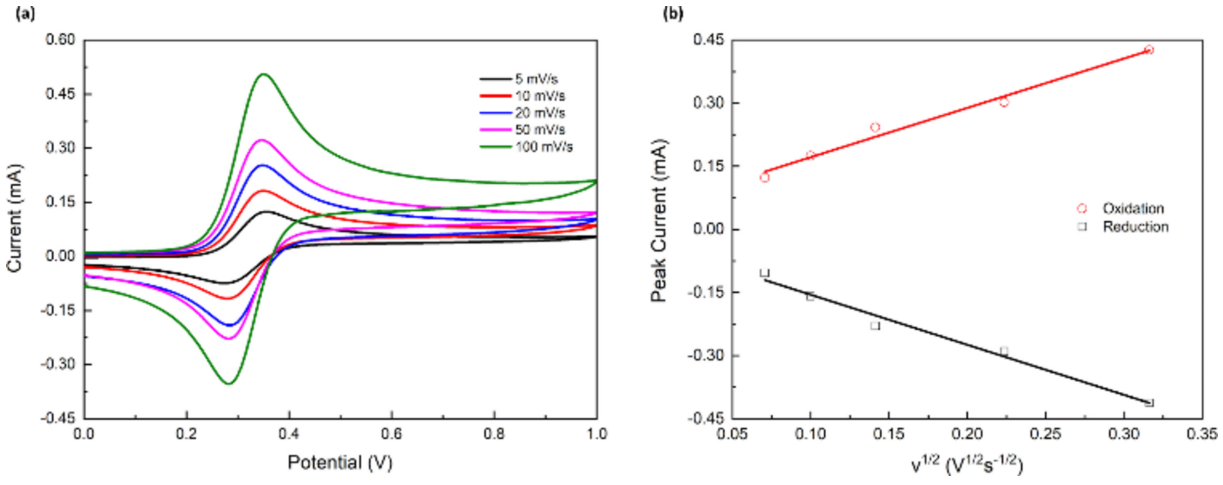

FIGURE 2 | (a) Comparison of different sweep rates from 5 to 100 mV/s, 25 mM 1,2,3-TAFc in 1 M HCl aqueous solution (pH = 0.4) (V vs. Ag/AgCl). (b) Randles–Ševčík analysis plots of the peak current versus the square root of the scan rates for 25 mM 1,2,3-TAFc.

TABLE 2 | Related data of Figure 3.

Concentration (mM)	Cathodic peak (mA)	Anodic peak (mA)	I_{PA}/I_{PC}	$E_{1/2}$ (V)	ΔE_p (mV)
2	−0.0690	0.0760	1.101	0.304	66
10	−0.1572	0.1629	1.036	0.308	61
25	−0.4120	0.4266	1.035	0.318	63

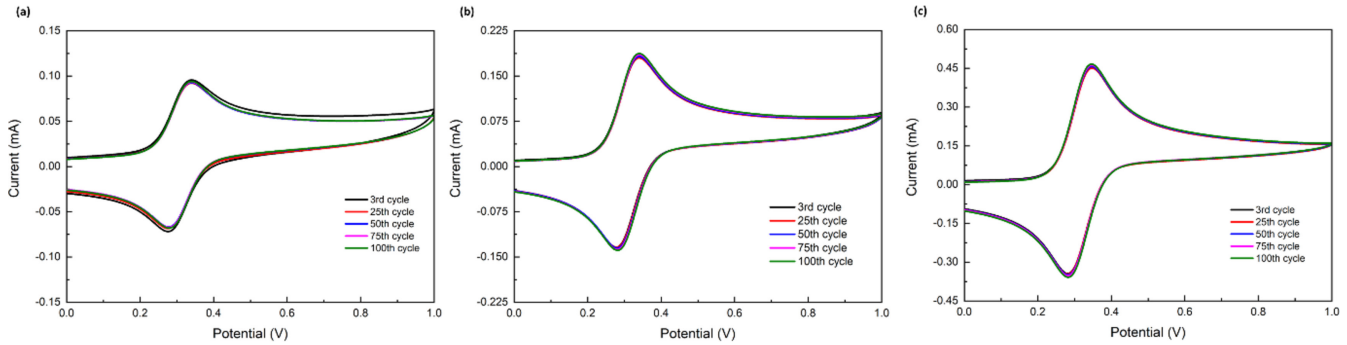

FIGURE 4 | (a) 2 mM, (b) 10 mM, and (c) 25 mM 1,2,3-TAFc in 1 M HCl aqueous solution (pH = 0.4) CV comparisons at the 3rd, 25th, 50th, 75th, and 100th cycles.

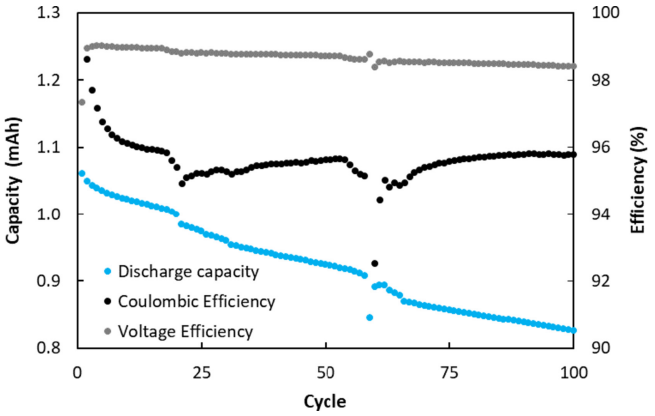

FIGURE 5 | Performance of 3 mM 1,2,3-TAFc battery in 1 M HCl + 1 M H_2SO_4 electrolyte CC cycling protocol.

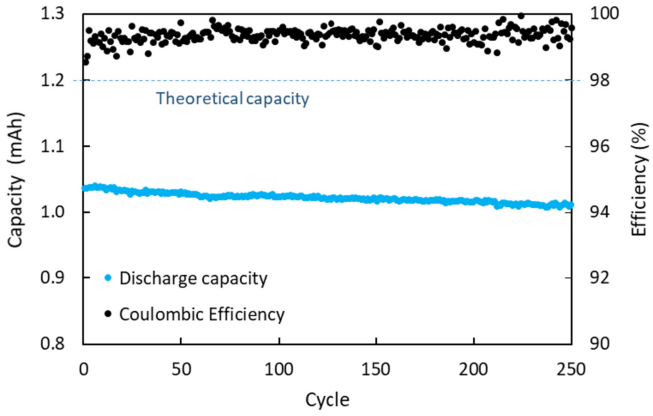

FIGURE 6 | Performance of 3 mM 1,2,3-TAFc battery in 1 M HCl + 1 M H_2SO_4 electrolyte CC + CV cycling protocol.

2.3 | Flow Battery Tests

Next, cycling tests in a lab-scale flow battery were conducted to investigate the stability of 1,2,3-TAFc. Cycling of the cell was performed with low concentration of 1,2,3-TAFc (3–10 mM) dissolved in an acidic electrolyte (mixture of 1 M HCl + 1 M H_2SO_4) as the positive electrolyte paired with excess of vanadium V^{3+} species dissolved in in the same supporting electrolyte. The CV comparisons of acidic electrolytes (HCl, H_2SO_4, and HCl + H_2SO_4) are depicted in Figure S4. The cell setup process, including internal images, is depicted in Figure S5.

We first assembled a battery with a 3 mM concentration of 1,2,3-TAFc and performed a constant current (CC) cycling. The cell was cycled for 100 cycles with low stability (0.221% capacity decay per cycle calculated over the 100 cycles). Additionally, sudden capacity decays around cycles 22 and 58 coupled with decrease in the Coulombic efficiency (Figure 5) was observed. These sudden capacity decays can be attributed to the adsorption of hydrogen atoms on the surface of the negative electrode, leading to a reduction in the active area and an increase in electrical resistance. This assumption is supported by the observation of gas bubbles on the negative electrode, as shown in Figure S5, indicating hydrogen gas evolution. The hydrogen evolution reaction not only consumes electrons, thereby reducing Coulombic efficiency, but also diminishes the activity of the vanadium couple on the negative electrode, contributing to the observed capacity deviations.

Next, we proceeded with cycling using a constant voltage (CV) protocol. This approach allows us to access the full available capacity while disregarding changes in internal resistance. The CV cycling at 0.95 V demonstrated higher stability of the system with low-capacity decay (0.011% per cycle, 3.0% per day) and higher Coulombic efficiency (99.4%) over 250 cycles (Figure 6).

Considering that this protocol minimizes the changes on the cell resistance, there is no noticeable cross-over of Fc to the

positive side and the posolyte consists on the stable couple V^{+3}/V^{+2} that is even in excess amount, we can attribute the measured capacity decay to 1,2,3-TAFc decomposition.

Finally, to investigate the increase on the cell resistance during cycling, we assembled a new battery with similar conditions and electrochemical impedance spectroscopy (EIS) was used to measure the resistance of the system before and after the test. The battery demonstrated the same behavior than the previous one when cycled using the CC protocol, with a high-capacity decay (0.201% per cycle) and decreasing voltage efficiency; furthermore, a similar faster decay was noticed around cycle 30. The impedance measurements, before and after the cycling, show that there is no change on the ohmic component, however an increase on the charge transfer resistance (Figure 7).

We attribute this to the adsorption of hydrogen atoms on the surface of the negative electrode, which lead to a reduction of the active area and an increase on the electrical resistance [27]. This assumption is supported by the formation of bubbles (Figure S6) on the negative electrolyte that suggests the evolution of hydrogen gas. Hydrogen evolution can account for the lower Coulombic efficiency of the cell, as some electrons are consumed in this reaction. Additionally, it contributes to diminishing the activity of the vanadium couple on the negative side.

3 | Experimental

3.1 | Chemistry

All reagents were obtained from commercial sources (Sigma-Aldrich and Boston Chemicals) and were used without further purification. Silica gel F254 (Merck 5554) precoated plates were used for thin layer chromatography (TLC) using UV light. ^{1}H NMR, ^{13}C NMR, and HSQC spectra were carried out using a 600 MHz Bruker NMR spectrometer at ambient temperature. FT-IR spectrum was recorded on the Nicolet-IS50 spectrometer. Absorbance of 2.10^{-5} M 1,2,3-TAFc solution in methanol was measured with an Agilent-CARY60 UV–Vis spectrophotometer. The melting point of 1,2,3-TAFc was recorded with an electrothermal digital melting points apparatus. HR-MS analysis was performed on Agilent 6530 Q-TOF LC/MS.

3.1.1 | General Procedure for the Synthesis of 1,2,3-TAFc

The solution of 2-bromoethylamine hydrochloride (408 mg, 2 mmol) and sodium azide (390 mg, 6 mmol) in 3 mL of water was stirred at room temperature for 10 min and then heated to 80°C for 5 h. The reaction progress was checked with thin layer chromatography (TLC), the reaction mixture was cooled to rt, and then 1.5 mL *t*-butanol, ethynylferrocene (273 mg, 1.3 mmol), $CuSO_4.5H_2O$ (33 mg, 0.13 mmol), and sodium ascorbate (52 mg, 0.26 mmol) were added. The reaction mixture was allowed to stir at room temperature for 10 h. After the reaction was completed, 2 M sodium hydroxide solution (20 mL) was added, and the mixture was extracted with chloroform (4 × 15 mL). The combined organic layers were dried over anhydrous sodium sulfate, filtered and concentrated under reduced pressure to yield a crude product, which was purified with column chromatography using a 2:1 methanol: chloroform solvent system.

Yield 73%, orange solid, mp 81°C–85°C. UV–Vis (λmax/nm, methanol): 443. FT-IR, ν, cm^{-1}: 3353, 3116, 2936, 1738, 1588, 1210, 1048, 816, 504, 482. ^{1}H NMR (600 MHz, $CDCl_3$, 25°C, TMS), δ, ppm: 7.54 (s, 1H), 4.70 (t, J = 1.2 Hz, 2H), 4.39 (t, J = 3.8 Hz, 2H), 4.28 (t, J = 0.8 Hz, 2H), 4.07 (s, 5H), 3.22 (t, J = 4.0 Hz, 2H), 1.49 (bs, 2H). ^{13}C NMR (151 MHz, $CDCl_3$, 25°C, TMS), δ, ppm: 146.83, 119.61, 75.51, 69.64, 68.74, 66.74, 53.46, 42.11. LC–MS/Q-TOF (m/z) calcd for $C_{16}H_{22}FeN_4$ $[M]^+$: 296.0724; found, 296.0735.

3.1.2 | Solubility Measurements of 1,2,3-TAFc

A fixed amount of the 1,2,3-TAFc was placed in a vial, and the appropriate solvent was injected until the 1,2,3-TAFc was completely dissolved. The maximal solubility was determined from the total amount of completely dissolved 1,2,3-TAFc [26].

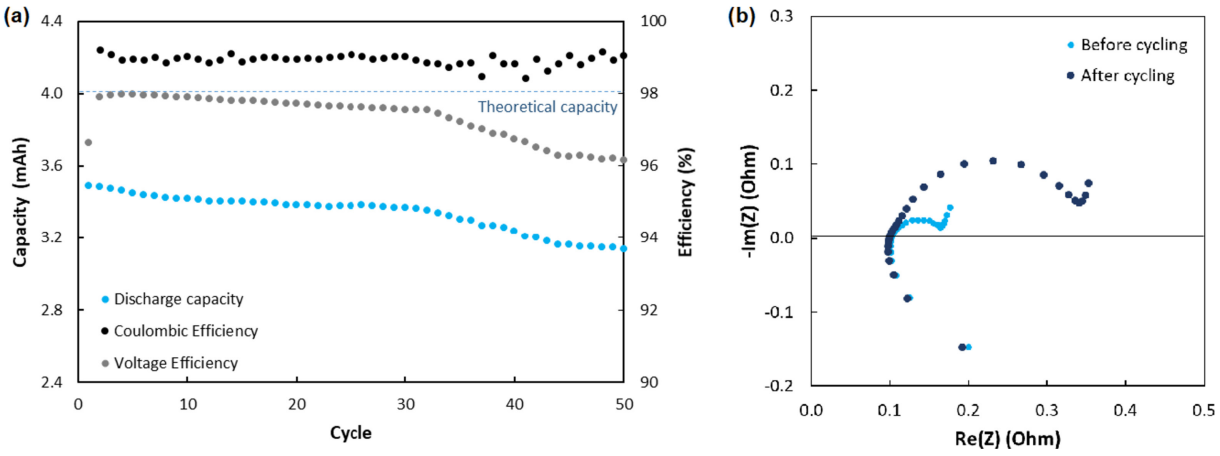

FIGURE 7 | 10 mM 1,2,3-TAFc battery in 1 M HCl + 1 M H_2SO_4 electrolyte using CC cycling protocol. (a) Battery performance. (b) EIS measurements before and after cycling.

3.2 | Cyclic Voltammetry (CV)

Electrochemical measurements were conducted using CH Instrument CHI608E model (CH Instruments Inc., Austin, TX/USA), Biologic SP-240 (BioLogic Sciences Inc., French), and Gamry Reference 600+(Gamry Instruments Inc., Warminster, PA/USA) potentiostats in a three-electrode glass cell over a wide range of electrode potentials (0 V to +1 V), scanning for potential positive electrode reactions at pH 0.4. A three-electrode glass cell with an electrolyte capacity of 5 mL was used; 1 M HCl solution was used as the supporting electrolyte. Glassy carbon (diameter: 0.30 cm) served as the working electrode. Silver-silver chloride (Ag/AgCl, 3 M KCl) and platinum wire were used as the reference and counter electrodes, respectively. All electrochemical measurements were performed under nitrogen atmosphere.

3.3 | Flow Battery Tests

In the cycling tests, a 5 cm^2 flow battery cell fabricated at the mechanical workshop of University of Turku equipped with flat flow fields was utilized. The cell consists of endplates (PVC), bipolar plates (fabricated from carbon composite plates from Pinflow ES, Czech Republic), and gaskets (3 mm thick expanded PTFE, cut from 24SH-ePTFE gasket sheets from TEADIT, Switzerland). Activated PAN carbon felts (GFD 4.65 EA) from SIGRACELL were employed. Proper membrane hydration was ensured by using the selected anion exchange membrane, Selemion DSVN from AGC Engineering, which had been soaked in deionized water for a minimum of 1 day before assembly. A peristaltic pump (Chonry BT600M) was calibrated using Masterflex C-Flex tubing from Cole-Parmer to provide a precise flow rate of 50 mL/min. The experiments were performed in a nitrogen-filled glovebox (MBRAUN). Battery performance measurements were conducted using a LANHE Battery tester 400 W. The electrolytes used in the glovebox batteries were prepared with deionized water and subjected to nitrogen purging and degassing before initiating the cycling tests. The supporting electrolyte consisted on a mixture of 1 M HCl + 1 M H_2SO_4. The dual electrolyte choice aimed to observe the influence of HCl on 1,2,3-TAFc. To ensure that the positive electrolyte was the limiting reactant, an excess of negative electrolyte was employed. Charging and discharging cutoffs were set at 0.9 and 0.6 V, respectively, in line with our experimental objectives.

3.3.1 | Flow Battery Tests Including PEIS Measurements

The flow-cell was assembled with a 10 mM concentration of 1,2,3-TAFc using the same conditions and acidic electrolyte (1 M HCl + 1 M H_2SO_4). The cycling was performed for over 50 cycles using a CC protocol to verify the same performance and resistance increase as in the previous cell. The resistance of the system was measured using potential electrochemical impedance spectroscopy (PEIS) with a Biologic SP-240 potentiostat.

4 | Conclusion

In summary, we have introduced a new type of Fc catholyte candidate for AOFBs based on a 1,2,3-triazole moiety. 1,2,3-TAFc was prepared easily via click chemistry with a one-pot, two steps reaction sequence with 73% overall yield. This is the first time that a 1,2,3-triazolium and an alkyl ammonium salt of Fc as a catholyte for AOFBs was investigated. 1,2,3-TAFc has 1.1 M solubility in 1 M HCl solution. The CV and flow battery experiments demonstrated the reversible and stable nature of the material. 1,2,3-TAFc may be the first member of a new Fc catholyte family as it can easily be converted to its water-soluble 1,2,3-triazolium or quaternary ammonium salts by simple alkylation reactions. 1- and 3-positions of the triazole ring are also suitable for derivatization to obtain ionic liquids of these species. The cycling battery tests show a high stability of this molecule in acidic electrolyte with low capacity decay (0.011%/cyc) and high Coulombic efficiency (99.4%). These results, which show the simple preparation, high solubility and stability of 1,2,3-TAFc, present this new molecule as a promising catholyte candidate for AOFBs. Flow battery performance and properties of ferrocene derivatives can be found in Tables S1 and S2.

Author Contributions

Taha Yasin Eken: investigation, methodology. **Gabriel Gonzalez:** investigation, methodology. **Pekka Peljo:** conceptualization, funding acquisition, writing – review and editing, writing – original draft, resources, supervision. **Gamze Koz:** conceptualization, writing – original draft, writing – review and editing, resources, supervision, funding acquisition.

Acknowledgments

We are grateful to the Bursa Technical University Scientific Research Fund (Project No. 231N002) for financial support. G. G. gratefully acknowledges the financial support from the University of Turku Graduate School. P. P. gratefully acknowledges the financial support from European Research Council Starting Grant (agreement no. 950038). This work partly utilized the Materials Research Infrastructure (MARI) at the University of Turku.

Conflicts of Interest

The authors declare no conflicts of interest.

Data Availability Statement

The data supporting this article have been included as part of the Supplementary Information.

References

1. J. P. Barton and D. G. Infield, "Energy Storage and Its Use With Intermittent Renewable Energy," *IEEE Transactions on Energy Conversion* 19 (2004): 441–448.

2. D. M. Kammen and D. A. Sunter, "City-Integrated Renewable Energy for Urban Sustainability," *Science* 352 (2016): 922–928.

3. J. Winsberg, T. Hagemann, T. Janoschka, M. D. Hager, and U. S. Schubert, "Redox-Flow Batteries: From Metals to Organic Redox-Active Materials," *Angewandte Chemie, International Edition* 56 (2017): 686–711.

4. R. F. Service, "Advances in Flow Batteries Promise Cheap Backup Power," *Science* 362 (2018): 508–509.

5. D. G. Kwabi, Y. Ji, and M. J. Aziz, "Electrolyte Lifetime in Aqueous Organic Redox Flow Batteries: A Critical Review," *Chemical Reviews* 120 (2020): 6467–6489.

6. G. L. Soloveichik, "Flow Batteries: Current Status and Trends," *Chemical Reviews* 115 (2015): 11533–11558.

7. J. Luo, B. Hu, M. Hu, Y. Zhao, and T. L. Liu, "Status and Prospects of Organic Redox Flow Batteries Toward Sustainable Energy Storage," *ACS Energy Letters* 4 (2019): 2220–2240.

8. B. Huskinson, M. P. Marshak, C. Suh, et al., "A Metal-Free Organic–Inorganic Aqueous Flow Battery," *Nature* 505 (2014): 195–198.

9. K. Lin, R. Gomez-Bombarelli, E. S. Beh, et al., "A Redox-Flow Battery With an Alloxazine-Based Organic Electrolyte," *Nature Energy* 1 (2016): 1–8.

10. A. Orita, M. G. Verde, M. Sakai, and Y. S. Meng, "A Biomimetic Redox Flow Battery Based on Flavin Mononucleotide," *Nature Communications* 7 (2016): 1–8.

11. B. Hu, C. Debruler, Z. Rhodes, and T. L. Liu, "Long-Cycling Aqueous Organic Redox Flow Battery (AORFB) Toward Sustainable and Safe Energy Storage," *Journal of the American Chemical Society* 139 (2017): 1207–1214.

12. A. Hollas, X. Wei, V. Murugesan, et al., "A Biomimetic High-Capacity Phenazine-Based Anolyte for Aqueous Organic Redox Flow Batteries," *Nature Energy* 3 (2018): 508–514.

13. E. S. Beh, D. De Porcellinis, R. L. Gracia, K. T. Xia, R. G. Gordon, and M. J. Aziz, "A Neutral pH Aqueous Organic–Organometallic Redox Flow Battery With Extremely High Capacity Retention," *ACS Energy Letters* 2 (2017): 639–644.

14. T. Janoschka, N. Martin, M. D. Hager, and U. S. Schubert, "An Aqueous Redox-Flow Battery With High Capacity and Power: The TEMPTMA/MV System," *Angewandte Chemie (International Ed. in English)* 55 (2016): 14427–14430.

15. Y. Liu, M. A. Goulet, L. Tong, et al., "A Long-Lifetime all-Organic Aqueous Flow Battery Utilizing TMAP-TEMPO Radical," *Chem* 5 (2019): 1861–1870.

16. Y. Zhao, Y. Ding, J. Song, et al., "Sustainable Electrical Energy Storage Through the Ferrocene/Ferrocenium Redox Reaction in Aprotic Electrolyte," *Angewandte Chemie (International Ed. in English)* 53 (2014): 11036–11040.

17. J. Yu, M. Salla, H. Zhang, et al., "A Robust Anionic Sulfonated Ferrocene Derivative for pH-Neutral Aqueous Flow Battery," *Energy Storage Materials* 29 (2020): 216–222.

18. B. R. Schrage, A. Frkonja-Kuczin, B. Zhang, et al., "Pyridinium Ferrocene Sulfonate Salts: Highly Soluble Materials for Electrochemical Applications," *Journal of Organometallic Chemistry* 991 (2023): 122695.

19. Z. Zhao, B. Zhang, B. R. Schrage, C. J. Ziegler, and A. Boika, "Investigations Into Aqueous Redox Flow Batteries Based on Ferrocene Bisulfonate," *ACS Applied Energy Materials* 3 (2020): 10270–10277.

20. B. R. Schrage, B. Zhang, S. C. Petrochko, et al., "Highly Soluble Imidazolium Ferrocene Bis(sulfonate) Salts for Redox Flow Battery Applications," *Inorganic Chemistry* 60 (2021): 10764–10771.

21. Q. Chen, Y. Li, Y. Liu, P. Sun, Z. Yang, and T. Xu, "Designer Ferrocene Catholyte for Aqueous Organic Flow Batteries," *ChemSusChem* 14 (2021): 1295–1301.

22. F. Himo, T. Lovell, R. Hilgraf, et al., "Copper(I)-catalyzed Synthesis of Azoles. DFT Study Predicts Unprecedented Reactivity and Intermediates," *Journal of the American Chemical Society* 127 (2005): 210–216.

23. A. J. Bard, L. R. Faulkner, and H. S. White, *Electrochemical Methods Fundamentals and Applications*, 3rd ed. (John Wiley & Sons, 2022).

24. Y. Li, Z. Xu, Y. Liu, et al., "Functioning Water-Insoluble Ferrocenes for Aqueous Organic Flow Battery via Host–Guest Inclusion," *ChemSusChem* 14 (2021): 745–752.

25. J. Luo, M. Hu, W. Wu, B. Yuan, and T. L. Liu, "Mechanistic Insights of Cycling Stability of Ferrocene Catholytes in Aqueous Redox Flow Batteries," *Energy & Environmental Science* 15 (2022): 1315–1324.

26. G. A. Mabbott, "An Introduction to Cyclic Voltammetry," *Journal of Chemical Education* 60 (1983): 697–702.

27. F. Chen, J. Liu, H. Chen, and C. Yan, "Study on Hydrogen Evolution Reaction at a Graphite Electrode in the All-Vanadium Redox Flow Battery," *International Journal of Electrochemical Science* 7 (2012): 3750–3764.

Supporting Information

Additional supporting information can be found online in the Supporting Information section.